Int J CARS (2016) 11:2173–2183
DOI 10.1007/s11548-016-1458-4

ORIGINAL ARTICLE

Feature detection in biological tissues using multi-band and narrow-band imaging

Yuki Tamura[1] · Tomohiro Mashita[1,2] · Yoshihiro Kuroda[3] · Kiyoshi Kiyokawa[1,2] · Haruo Takemura[1,2]

Received: 12 January 2016 / Accepted: 1 July 2016 / Published online: 14 July 2016

Abstract
Purpose In the past decade, augmented reality systems have been expected to support surgical operations by making it possible to view invisible objects that are inside or occluded by the skull, hands, or organs. However, the properties of biological tissues that are non-rigid and featureless require a large number of distributed features to track the movement of tissues in detail.
Methods With the goal of increasing the number of feature points in organ tracking, we propose a feature detection using multi-band and narrow-band imaging and a new band selection method. The depth of light penetration into an object depends on the wavelength of light based on optical characteristics. We applied typical feature detectors to detect feature points using three selected bands in a human hand. To consider surgical situations, we applied our method to a chicken liver with a variety of light conditions.
Results Our experimental results revealed that the image of each band exhibited a different distribution of feature points. In addition, the total number of feature points determined by the proposed method exceeded that of the R, G, and B images obtained using a normal camera. The results using a chicken liver with various light sources and intensities also show different distributions with each selected band.
Conclusions We have proposed a feature detection method using multi-band and narrow-band imaging and a band selection method. The results of our experiments confirmed that the proposed method increased the number of distributed feature points. The proposed method was also effective for different light conditions.

Keywords Multi-band imaging · Narrow-band imaging · Biological tissues · Feature detection · Augmented reality

This work was partly supported by JSPS KAKENHI Grant Number 26282147. The study was approved by the Ethical Review of the Faculty Meeting of Cybermedia Center, Osaka University, Japan.

✉ Yuki Tamura
tamura.yuuki@lab.ime.cmc.osaka-u.ac.jp

1 Graduate School of Information Science and Technology, Osaka University, 1-5 Yamadaoka, Suita City, Osaka 565-0871, Japan

2 Cybermedia Center, Osaka University, 1-32 Machikaneyamacho, Toyonaka City, Osaka 560-0043, Japan

3 Graduate School of Engineering Science, Osaka University, 1-3 Machikaneyama-cho, Toyonaka City, Osaka 560-8531, Japan

Introduction

Dense feature detection of biological tissues is important for augmented reality (AR) navigation systems, which are expected to support surgical operations by making it possible to view invisible objects inside or occluded by the skull, hands, or organs [1]. In general, human tissues are non-rigid and deform during surgery, including the cerebrum, hands, and internal organs. For example, the skin of a human hand deforms during syndactyly surgery, and the skin displacement is important information for augmenting images of the arteries running along the fingers to avoid damaging them.

AR navigation systems require pairs of corresponding points between two images to estimate the displacement of the points' three-dimensional (3D) positions. To deal with local deformation of an object in the navigation, dense features are required. The number and the spatial distribution of feature points are both important because feature points with similar positions are meaningless. The purpose of this study is to develop a feature detection system to obtain dense features from biological tissues.

We focus on how the depth of light penetration depends on wavelength. Short-band light is reflected or scattered on the surface or a shallow area of the biological tissue, while long-band light can penetrate more deeply. Therefore, each light band reflects the structure at a different depth of the tissue. To obtain more feature points from tissues, we take advantage of the properties of the illumination related to light bands. Narrow-band imaging (NBI) has been proposed for visualizing abnormal tissue for clinical use [2]. However, to the best of our knowledge, this method has never been applied for feature detection.

In this study, we propose a novel feature detection system with multi-band and NBI (multi-NBI) for biological tissues. In particular, we developed an NBI system consisting of a tunable filter and a high-sensitivity camera. We also designed a method of band selection for efficient measurements. We examined both the number and spatial distribution of detected features with a human hand, which is one of the target biological tissues of AR navigation. In addition, the effects of the types and intensities of light sources are also considered.

Related work

Conventional NBI uses the absorption peaks of hemoglobin at light wavelength of 415 and 540 nm. Sano et al. [2] enhanced the microstructures of the superficial mucosal layer using NBI. However, this technique is designed to find a tumor by visualizing the concentration of vessels; it is not designed to detect feature points. On the other hand, NBI can enhance a certain feature by limiting the wavelength band.

The properties of illumination have been studied to obtain surface and subsurface information about objects. Nayar et al. [3] proposed a method that separates an image into global and direct components. The global component of illumination is the light that passes through another medium, such as subsurface scattering. The direct component is derived directly from the light source and obtained by removing the global component. In the method by Nayar et al., high-frequency illumination patterns are projected onto a scene, and then the two components are generated from the images. Tanaka et al. [4] applied this method to a translucent object. This method yields sliced images of the area within the tissue. However, it is difficult to apply this method to AR surgery because it takes too much time to obtain the two components by projecting high-frequency illumination patterns. In addition, more feature points from a scene are required, but sliced images at each depth are not needed for our purpose.

Near-infrared (NIR) imaging is a beneficial tool for detecting a foreign substance under skin. Hayakawa et al. [5] used NIR light imaging to detect a foreign substance under skin. Nishida et al. [6] improved the transillumination image of blood vessels using multi-band light. In this study, we use visible light instead of NIR, because short wavelengths can enhance surface structure.

To detect features and track tissues, Elhawary and Popovic [7] proposed a combination of the Speeded-Up Robust Features (SURF) feature descriptor [8] and the Lucas–Kanade tracking method [9]. This combination is robust for tracking heart motion in real time. Haouchine et al. [10] also adapted this combination for liver tracking with a stereo endoscope, but they did not focus on improving feature detection for biological tissues. In this study, we focus on feature detection.

Feature detection using multi-band imaging and NBI

Concepts

Using multi-NBI, it is possible to obtain more feature points from different wavelength images. However, the results are useless if the positions of the detected features are the same between the band images. Therefore, it is important to obtain different distributions of feature points from the band images. In addition, the measurement should run efficiently for surgical navigation, and the measurement time increases with the number of band images.

Figure 1 illustrates the concept of the proposed system. The particular narrow-band of the reflected light passes through the filter and is captured using a high-sensitivity camera. The filter and camera are controlled by a personal computer. If each band image has a different distribution of feature points, the total number of feature points essentially increases.

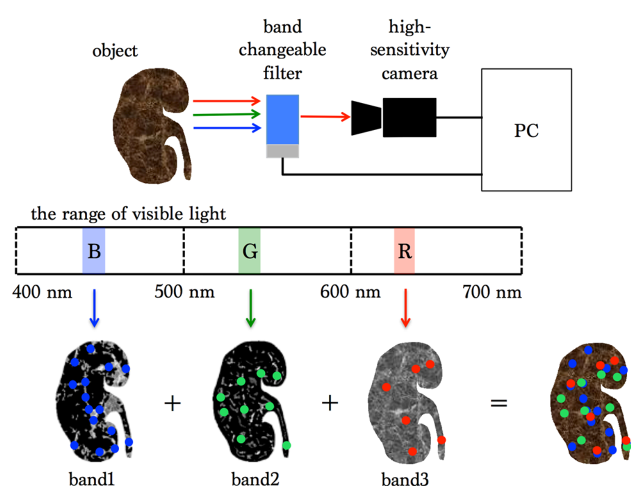

Fig. 1 Concept of the proposed system. The *colored points* at the *bottom* are examples of feature points from each band image

Band selection

Because capturing all available band images requires too much time, band selection is a key feature of the proposed system for efficient processing. We accordingly introduced a criterion to select several remarkable bands to detect feature points.

We calculated the variation ratio $Q(n, m)$ between two bands n and m of images using the following equations:

$$P(x, y) = \left| \frac{\mathrm{d}I_n(x, y)}{\mathrm{d}n} \right|, \tag{1}$$

$$P_{nm}(x, y) = \left| \frac{I_n(x, y) - I_m(x, y)}{n - m} \right|, \tag{2}$$

$$Q(n, m) = \frac{1}{w \times h} \left(\sum_{i \in w} \sum_{j \in h} P_{nm}(i, j) \right), \tag{3}$$

where $I_n(x, y)$ is the pixel value of the coordinates (x, y) of a band n image, $P(x, y)$ is the variation of intensity between two bands, $Q(n, m)$ is the average of $P(x, y)$, and w and h are the image's width and height, respectively. In this study, we examined wavelengths in the range of 400–720 nm.

In the case of large $Q(n, m)$, the appearances of bands n and m are significantly different, which indicates that these bands exhibit different features. In this work, the difference of bands to compare is fixed to a constant k. We accordingly calculated $Q(n, n + k)$ within the range of wavelengths. We selected bands using the following conditional equations:

$$Q(n - k, n) < Q(n, n + k), \tag{4}$$

$$Q(n + k, n + 2k) < Q(n, n + k). \tag{5}$$

We selected three bands to compare the performance with the R, G, and B images of a normal camera. We selected two sets in which $Q(n, n + k)$ is large and satisfies the above conditions. If $Q(n_1, n_1 + k)$ and $Q(n_2, n_2 + k)$ are selected as $(n_1 < n_2)$, there are three different intensity regions: (a) wavelengths of n_1 or less, (b) between $n_1 + k$ and n_2, and (c) $n_2 + k$ and longer. Then, n_1 from (a), $n_2 + 2k$ from (c), and $\frac{n_1+n_2+2k}{2}$ from (b) were selected.

To detect feature points, we used the scale-invariant feature transform (SIFT) [11], which performs better than SURF. SIFT is robust for image rotation, scale, and light environments, and it has been used for feature detection, tracking, and matching in many cases of image processing. However, SIFT is associated with a high computational cost. Features from Accelerated Segment Test (FAST) is another representative feature detector, which detects corners in an image [12]. For comparative evaluation of features, we tested SIFT, SURF, and FAST.

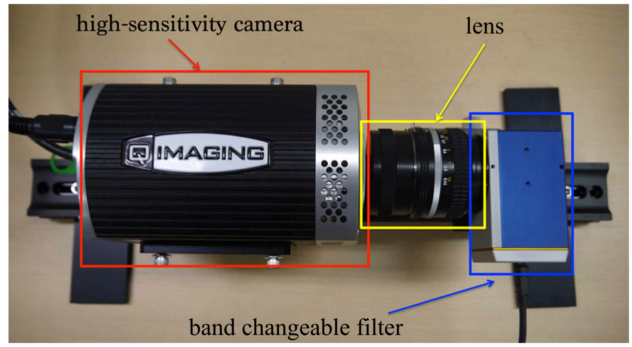

Fig. 2 Our multi-band imaging and NBI system

Evaluation

System configuration

Figure 2 shows the implemented system based on the noted requirements. We used a VariSpec™ liquid crystal tunable filter (CRi) as a controllable narrow-band filter. This device filters in increments of 10 nm over a range of 400–720 nm, and a setting band with ±5 nm is filtered. Due to the low light intensity during filtering, we used an optiMOS camera (QImaging) with a high-sensitivity image sensor, a resolution of 1920 × 1080 pixels, and a maximum frame rate of 100 fps. The camera and filter were controlled using a personal computer (Windows 7, 64 bit, Intel Core i7-4790k at 4.00 GHz, 16 GB memory, and NVIDIA GeForce GTX 760 graphics card). We implemented the program to control the camera and filter in C++, and OpenCV 2.4.9 was used to detect features. We used each feature detector with the default threshold values in OpenCV.

Our prototype system ran at approximately 20 fps due to the high resolution, and our light source was an LP-500U white LED (FalconEyes). We used a human hand, which is one of the target tissues of AR surgery and a biological tissue that can be captured consistently under a variety of conditions for a long time. We also demonstrate how this procedure works with a chicken liver.

Feature point distribution

As a result of the band selection in Fig. 3, we computed two sets, $n_1 = 450$ and $n_2 = 590$. Then, we obtained 450, 530, and 610 nm as the selected bands. We defined $k = 10$ heuristically in Eqs. 4 and 5 and selected three bands.

Figure 4 shows examples of the images captured by our imaging system and the spatial distribution of the feature points with SIFT, SURF, and FAST. The image of the short band in Fig. 4a shows surface wrinkles and spots. In contrast, the image of the long band shows blood vessels, although the image is textureless. Each channel of the normal camera

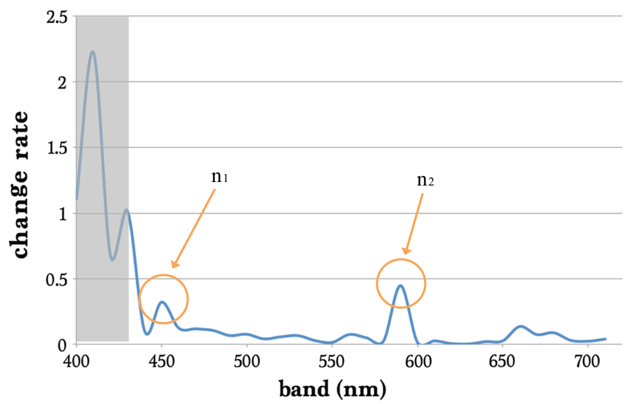

Fig. 3 Results of the band selection. We excluded images with wavelengths below 430 nm (*gray area*) from the band selection because this wavelength range exhibited significant noise level due to the low light intensity based on the light source's spectral characteristics

image includes a much wider wavelength range compared to the proposed narrow-band image. The wider band would hide the features specific to a certain wavelength.

Figure 5 shows normal camera images and the spatial distribution of the feature points. We used Point-Grey FL2-08S2C-C (with 1032×776 pixels and 30 fps) to obtain normal RGB images. We observed blood vessels with increasing wavelength (from the B channel to the R channel), but the changes were less pronounced than in the narrow-band images.

The lower three rows of Fig. 4 show the spatial distribution of feature points with SIFT, SURF, and FAST. In general, the numbers of feature points at 450 nm in Fig. 4d1, e1, f1 are greater than those of the other band light images. As the bands become wider, the number of feature points decreases because it is difficult to obtain a clear image in strong scattering at a long wavelength. In the case of normal camera

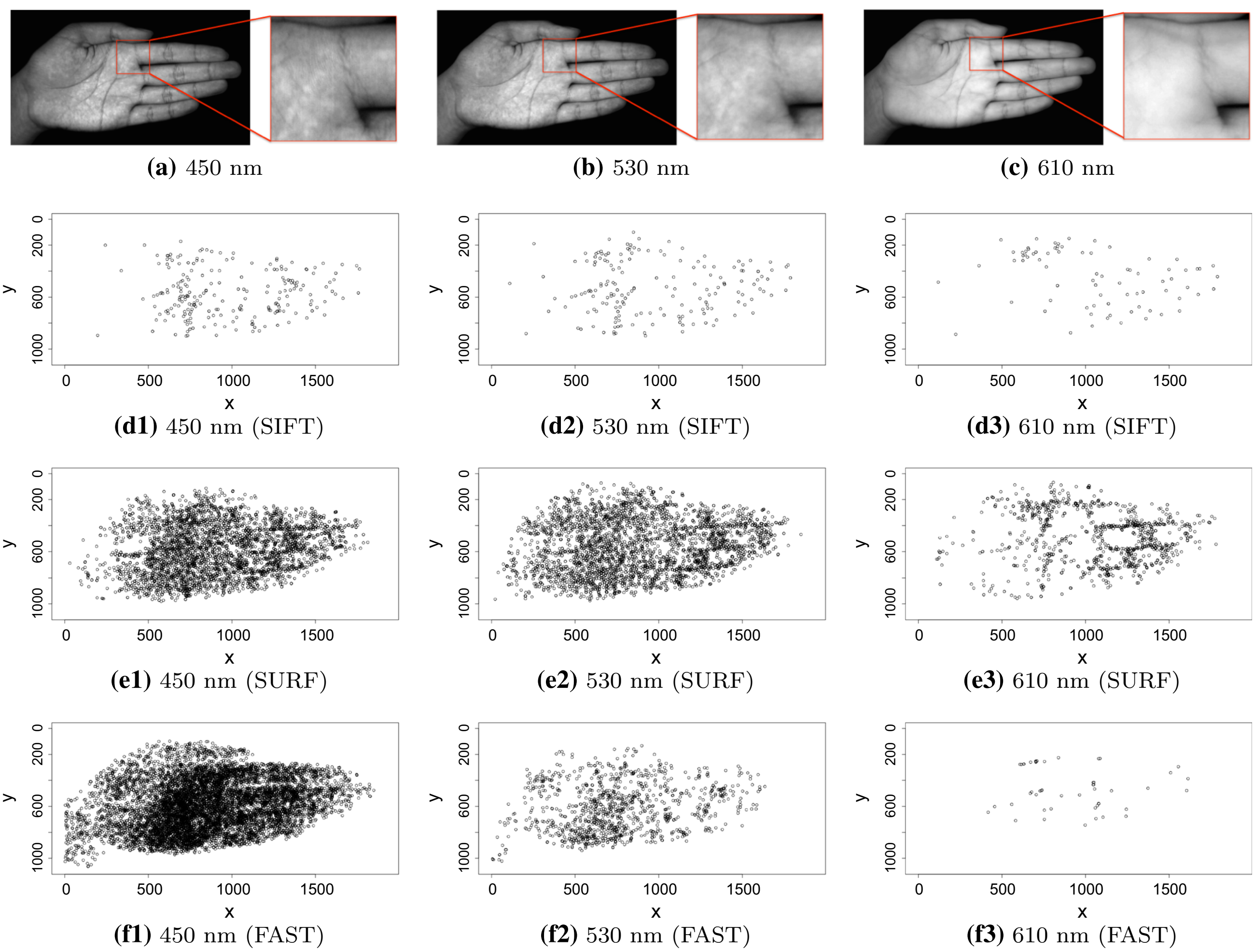

Fig. 4 Example of narrow-band images. The *top row* shows examples, while the *lower three rows* show the spatial distribution of the feature points with SIFT, SURF, and FAST. The image of the short-wavelength band (*left*) includes spatially high-frequency features, wrinkles, and mottles. In the long-wavelength band, spatially low-frequency features, blood vessels, and deep wrinkles appear (*right*). The feature points of the short-wavelength band are denser than the feature points of the long-wavelength band

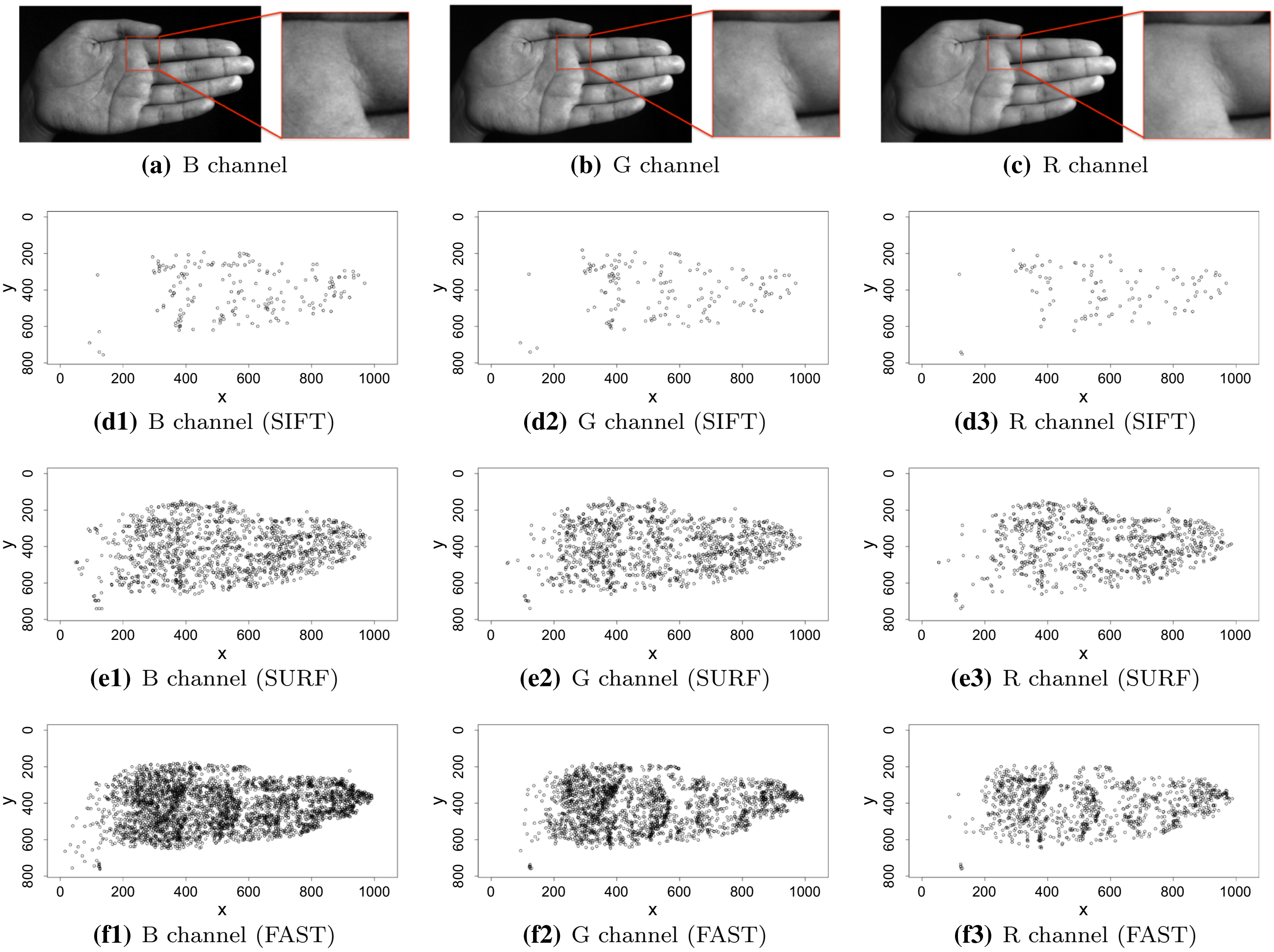

Fig. 5 Normal camera images (RGB channel). The *top row* shows each channel of images, and the *lower three rows* show the spatial distribution of the feature points with SIFT, SURF, and FAST

images, the lower three rows from (d1) to (f3) of Fig. 5 show that the numbers of feature points in the B channel in Fig. 5d1, e1, f1 are greater than those in the other channels.

To evaluate these feature point distributions, we applied a hierarchical cluster analysis that assembles hierarchical clusters based on the similarity of particular components. We used the average and the deviation of all feature point coordinates as input data. Figure 6 shows the result of the clustering dendrogram with SIFT features, in which the height signifies the distance between two clusters. A lower hierarchy in the tree implies that the components of the cluster are closer than those of a higher hierarchy. According to Fig. 6, if we use the largest cluster (i.e., a tree height of 1000), then there is a boundary between 580 and 600 nm. When we select the cluster at a tree height of 300, there are three clusters, and our selected bands (450, 530, and 610 nm) are clustered separately. In addition, the analysis results of feature points detected with SURF and FAST were similar to the clustering result using SIFT, and the largest cluster boundary was between 580 and 600 nm. In the case of SURF, we needed five clusters to separate the selected band into different clusters. The similarity of clusters increased somewhat, and there is another cluster with different distributions. In the case of FAST, we needed three clusters to separate the selected bands, which was the same as SIFT. Therefore, the proposed method was also effective for different light conditions.

Number of feature points

To verify the efficiency of feature detection with NBI, we compared three types of images: narrow-band images from our system, synthesized normal-band images, and images obtained with a normal camera. The synthesized images represented the weighted sum of multi-NBI in which the weighting parameters were determined by referring to the normal camera's spectral sensitivity. To compare the number of feature points in each type of image, we conducted two-way analysis of variance with multiple comparisons using the Holm–Bonferroni method. The first factor is the type of

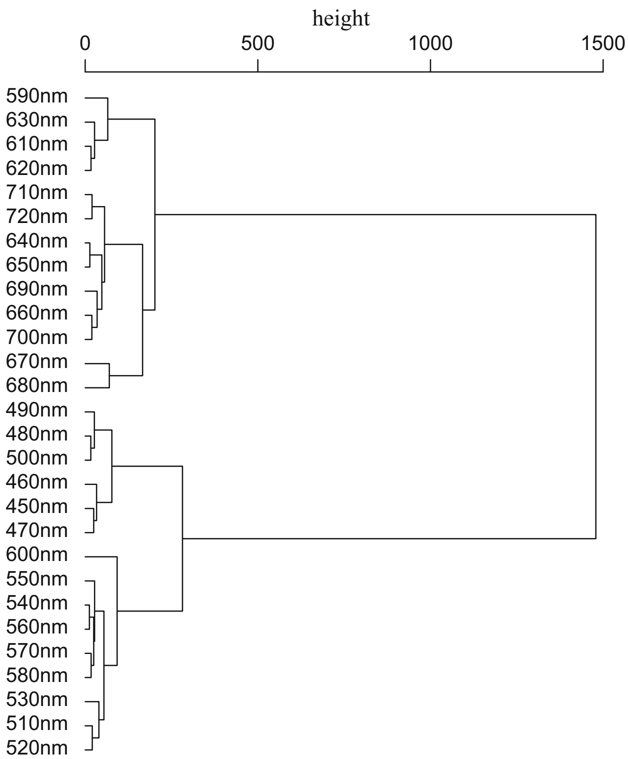

Fig. 6 Hierarchical cluster analysis dendrogram of a human hand with SIFT feature points distribution

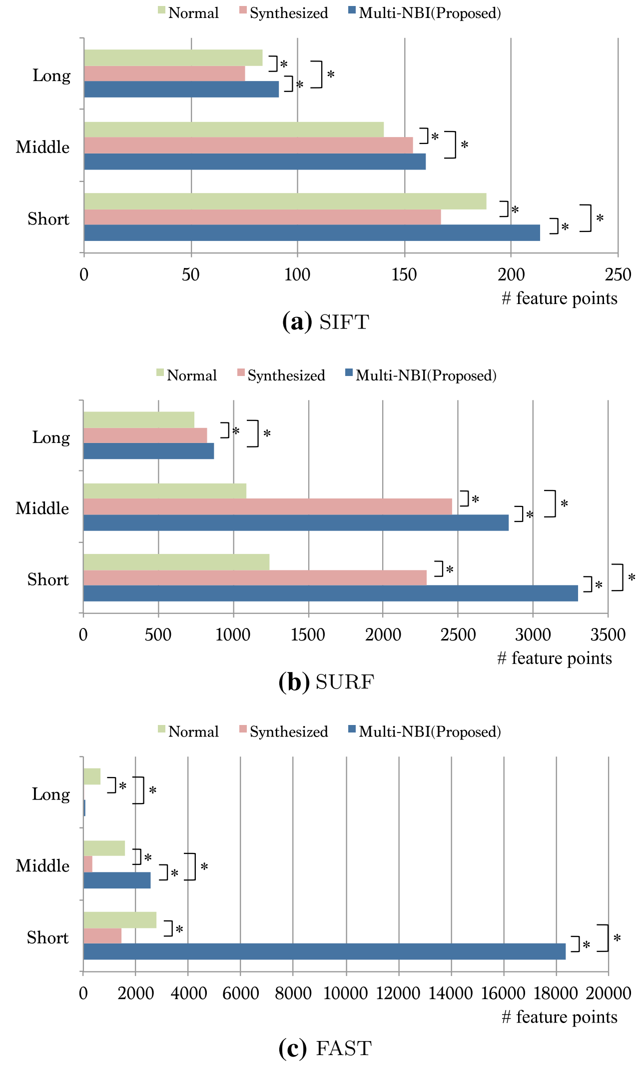

Fig. 7 Number of feature points of three different band images using a normal camera, synthesized image, and the narrow-band images with SIFT, SURF, and FAST

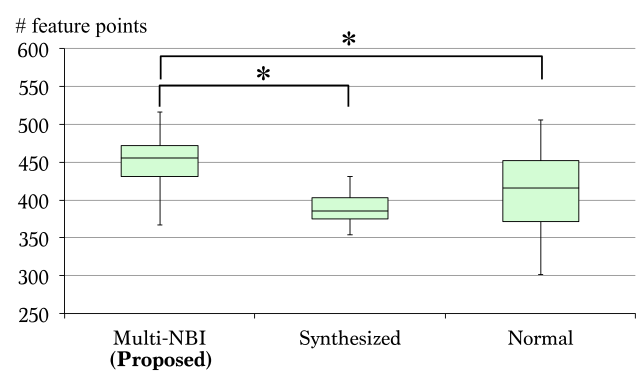

Fig. 8 The sum of feature points of a normal camera, synthesized image, and the narrow-band images with SIFT

image noted above, and the second factor is the band. In this comparison, the bands for NBI are 450 nm (short), 530 nm (middle), and 610 nm (long), which correspond to the blue, green, and red channels of a normal camera, respectively. Similar to the previous evaluation, we used a human hand as a sample, and we captured 20 samples in various postures from one person.

Figure 7 shows the results of multiple comparisons of different types of images. We observed significant differences between the G and B images obtained with a normal camera and those obtained with narrow-band images at 530 and 610 nm, respectively. However, the comparison of the long band gave a different result. This is because FAST is a corner detection method, but the long-band image is not a clear image and has a small number of corners. The improvement in the synthesized images is limited or in some cases nonexistent. In addition, we compared the sum of the feature points in the R, G, and B images with the sum of feature points of the multi-NBI images (450, 530, and 610 nm) with SIFT, as shown in Fig. 8. We found significant differences between the sum of feature points in the images from the normal camera and the multi-NBI images ($p < 0.005$). We can accordingly conclude that the number of detected feature points in the narrow-band images is greater than the feature points detected by the normal camera, except for the shortest band. Moreover, the sum of feature points using the narrow-band data exceeded that of the normal camera. These results showed that our method was effective in typical feature detectors. A proper feature detector should be chosen according to the purpose of use. For example, since FAST mainly detects corners, it is inappropriate for biological tissues, which have uniform texture and few corners.

Application to another tissue and the effects of types and intensities of light sources

We next analyzed how the proposed method works for feature detection using chicken liver tissue. We obtained a chicken liver that was being sold for consumption, and we used it for experiments ex vivo. Thus, there were no ethical issues.

We tested the proposed method in a variety of illumination conditions that might occur in surgical situations. For this purpose, we used a PCS-UHX-AIR halogen light (Optical Garden) and the aforementioned white LED light as light sources. We measured an object while changing three intensity levels of each light source. For example, the intensity of LED2 is stronger than that of LED1, and that of LED3 is stronger than that of LED2. The exposure time was 20 ms. Figure 9 shows the spectrum of each light source.

We captured chicken liver images in increments of 10 nm over a range of 400–720 nm. Table 1 shows the result of band selection with each light source intensity. The pixel value changed with the types and intensities of light sources, which is exploited by our method. Therefore, the selected bands were different among the different light conditions.

Figure 10 shows the images with the selected bands listed in Table 1. In this experiment, we analyzed the images with SIFT only because the main focus is to analyze the effects of the light source conditions. Figure 11 shows the SIFT feature point distribution of Fig. 10 images. Overall, the distributions of feature points varied visually from the short band to the long band. However, similar to the "Feature Point Distribution" section, the distributions of feature points analyzed by hierarchal clustering showed no division of the selected band into different clusters when we cut it into five clusters. This probably occurred because the short- and long-band images have similar intensities and thus similar spatial distributions.

Discussion

We have confirmed that the proposed system makes it possible to detect a greater number of distributed feature points from a human hand. However, the number of feature points was not significantly different between the normal camera and the proposed multi-NBI in short bands, as shown in Fig. 7. This finding may be caused by the limited reflection of light due to the absorption of short-band light in the tissue. Moreover, multi-NBI could not detect the lesion because the band it selected was not necessarily the band strongly absorbed by hemoglobin. To enhance the lesion area, we must select the absorption peaks of hemoglobin at 415 and 540 nm. However, we focused on obtaining different distributions of feature points. Thus, it is not necessary to select these bands.

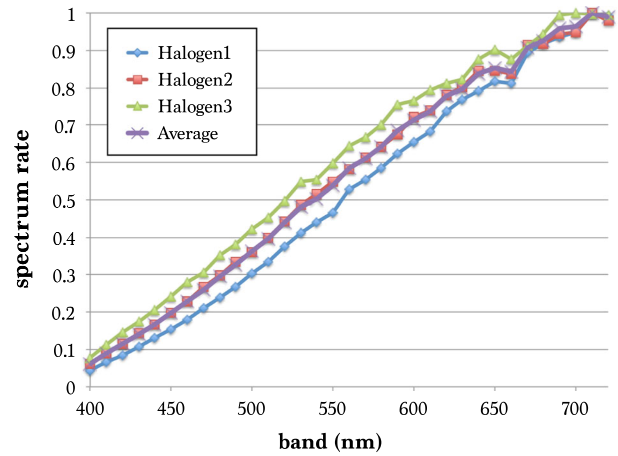

(a) Halogen light spectrum

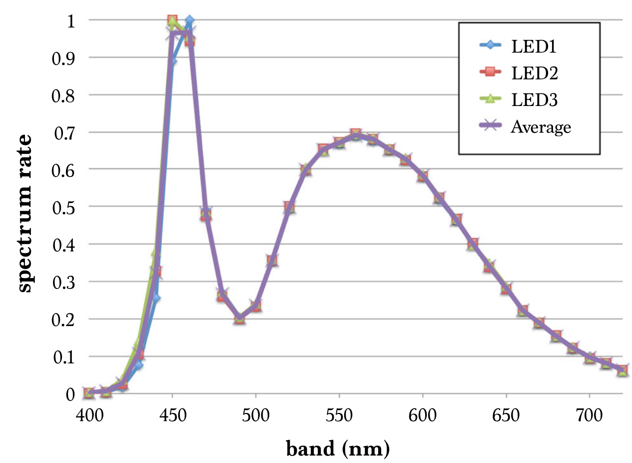

(b) LED light spectrum

Fig. 9 Light source spectrum normalized by maximum value of each light conditions. The maximum value of the vertical axis is one

Table 1 Band selection and clustering results for different intensity levels for each light source

	Short (nm)	Middle (nm)	Long (nm)	Cluster
Halogen				
1	510	540	570	8
2	510	530	560	11
3	470	540	610	8
LED				
1	470	520	570	16
2	480	580	680	4
3	490	540	600	5

Halogen1 is weaker than Halogen2, and Halogen2 is weaker than Halogen3. The same order applies to the LEDs. "Cluster" means the number of clusters needed when dividing the three bands

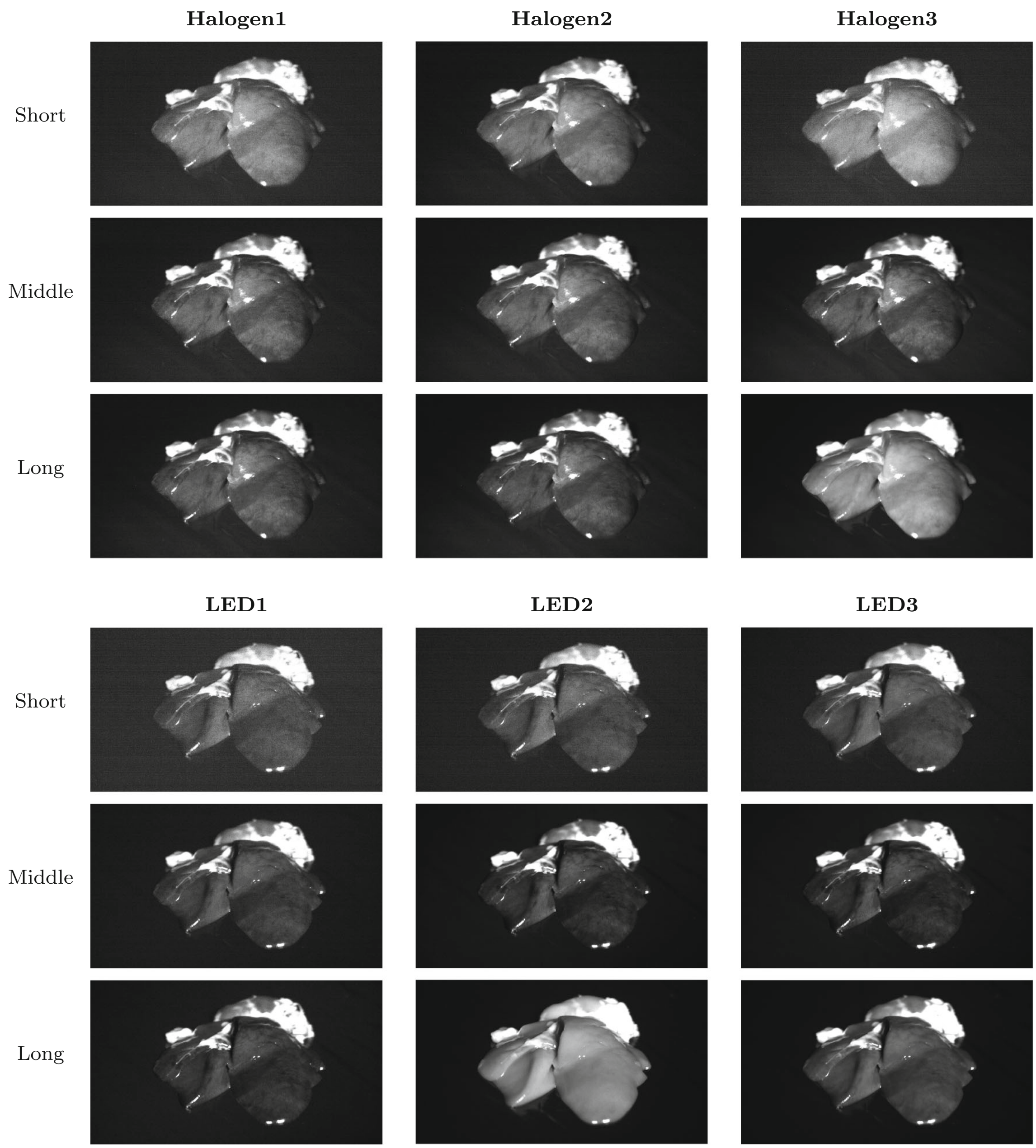

Fig. 10 Results of measuring chicken liver at different intensity levels for each light source. Short, middle, and long mean the selected band listed in Table 1 for each condition

In order to apply the method to a case of AR surgery, the tracking performance and robustness under deformation must be verified. However, since our approach using the multi-NBI images is theoretically independent of the feature detector and tracking algorithm, our findings are meaningful. In the future, we would like to apply the method under the situations noted to verify its performance. In addition, this work only focused on image processing and feature detection. Application to AR surgery, however, requires an accurate tracking algorithm for features detected by our method. For example, Souza et al. [13] proposed a feature matching algorithm for surgical images, which are the following steps of our part. It would be possible to apply Souza's method to the feature points obtained by our multi-NBI method for tracking.

We used SIFT, SURF, and FAST for detecting feature points. SIFT is associated with a high computational cost, so we need to use a faster detector such as SURF or FAST for testing in real time, and we must also consider parallel processing using a GPU. In addition, SIFT is a feature descriptor that is invariant of image rotation, image scaling, and light illumination. SIFT is also robust to global bright-

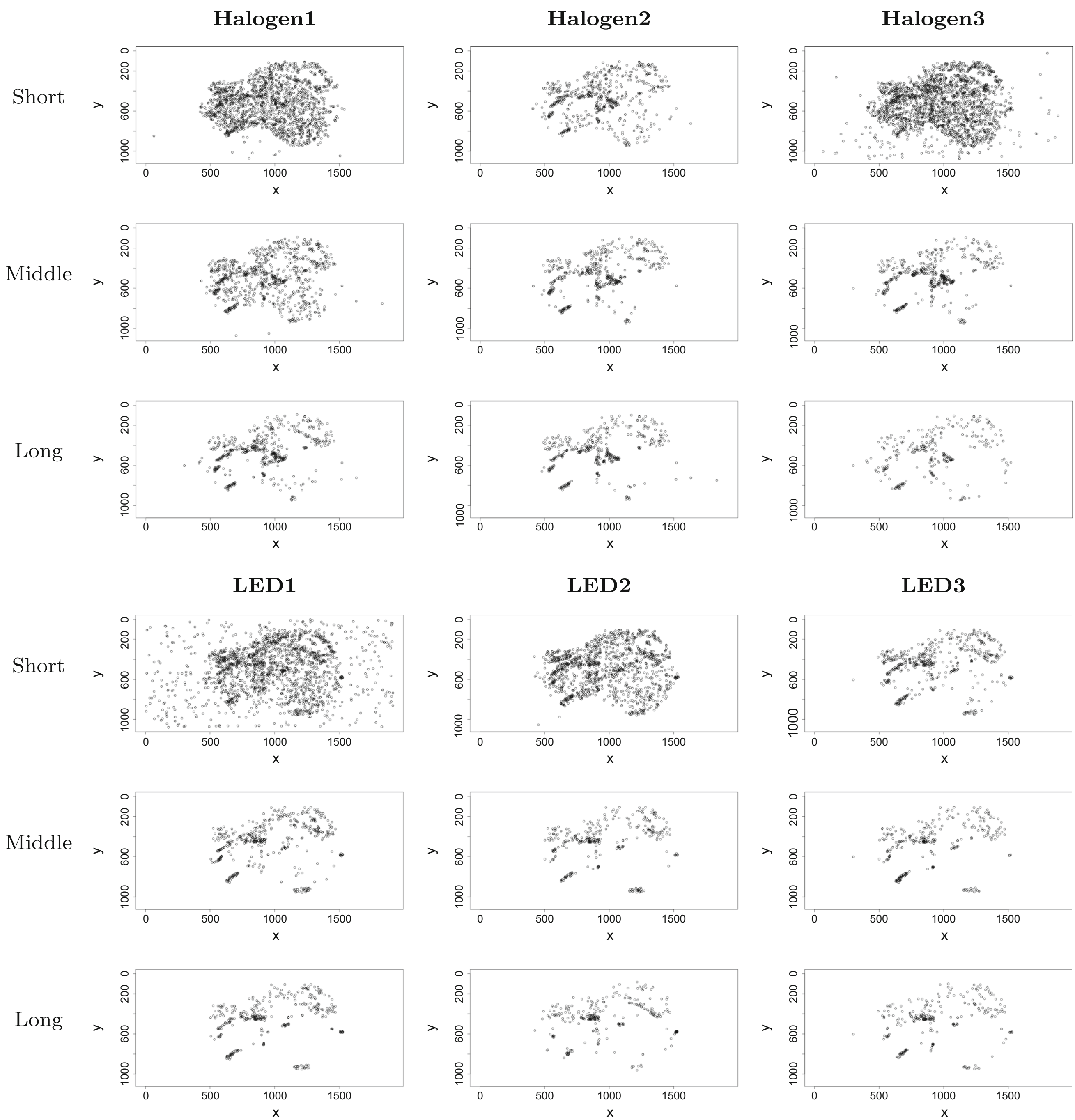

Fig. 11 Distributions of feature points with SIFT applied to Fig. 10 images

ness changes but not to local changes. On the other hand, SIFT is not robust to deformation. Recently, Ling et al. [14] proposed a local descriptor that is invariant to deformation using geodesic-intensity histograms. In addition, Lobaton et al. [15] proposed a local descriptor that is invariant to locally bounded deformations using homology. In the future, we will evaluate the proposed method under deformation using techniques such as these.

The results of the ex vivo experiment with a chicken liver might be different from in vivo and in vitro results. There is no blood flow in the case of an ex vivo experiment. It was expected that the measurement with a particular light band would make a difference because the peaks of light absorption of hemoglobin in blood vessels are 415 and 540 nm. Even in vitro results would show differences from in vivo results. Therefore, investigating the differences between

Table 2 Band selection and clustering results of intensity levels for each light source with modified band selection

	Short (nm)	Middle (nm)	Long (nm)	Cluster
Halogen				
1	510	610	710	4
2	540	620	700	7
3	470	510	550	12
LED				
1	470	590	710	5
2	480	580	680	4
3	490	580	680	4

in vivo, in vitro, and ex vivo is one of topics for future work.

The captured image depends on the light source's properties, intensity levels, and the camera and lens parameters (aperture stop, focus, shutter speed, and so on). Depending on the type of light source, there is a band that does not emit strong light, particularly a short band. Thus, if the exposure time is short, it is impossible to obtain a clear image. This problem has not been solved with contrast adjustment. If we apply contrast adjustment, image noise is enhanced, and the fine texture of the short band is lost. On the other hand, saturation occurs if the exposure time is long or the light intensity is strong in the case of the long band. Therefore, for each band, it could be useful to set an appropriate exposure time and system parameters.

As mentioned, we obtained worse hierarchical clustering results for feature point distributions with a chicken liver compared to a human hand. This was particularly apparent for LED3, as shown in Fig. 10. The short- and long-band images had similar intensities, and it was possible to detect similar distributions of feature points. To deal with this problem, we added a constraint to the band selection method, which chooses the bands n_1 and $n_2 + 2k$, for which images have a large difference in intensity. This constraint guarantees that the short- and long-band image intensities will be different. Table 2 shows the band selection results with the modified band selection method. The results of this modification showed great improvement in the clustering analysis. In addition, when we applied this constraint method to human hand images, we obtained the same band selection result. We thus concluded that the modified band selection method was effective in terms of the distribution of feature points.

Conclusion

We have proposed a feature detection method using multi-NBI and band selection. We implemented our system using a variable band filter and a high-sensitivity camera. Our experimental results using a human hand revealed differences in terms of intensity and the spatial distribution of the feature points according to the band selection method. There were more feature points in multi-NBI images than in normal camera images. This effect persisted in all bands with the exception of the shortest band, and the total number of feature points was also greater. We also found a different appearance and distribution of feature points when we applied the proposed method to a chicken liver with various types and intensities of light sources. Based on these results, we can conclude that the proposed multi-NBI feature detection method with the intensity constraint increased the number of feature points that have different spatial distributions. It will be valuable to test this methodology using other biological tissues inside a body in future studies. Follow-up work should include an evaluation of the proposed method in terms of tracking performance under deformation by measuring an organ in surgical situations.

Compliance with ethical standards

Conflicts of interest We have no conflicts of interest relationship with any companies or commercial organizations based on the definition of the Japanese Society of Medical and Biological Engineering.

References

1. Hashizume M, Yasunaga T, Tanoue K, Ieiri S, Konishi K, Kishi K, Nakamoto H, Ikeda D, Sakuma I, Fujie M, Dohi T (2008) New real-time MR image-guided surgical robotic system for minimally invasive precision surgery. Int J Comput Assist Radiol Surg 2:317–325
2. Sano Y, Emura F, Ikematsu, H (2009) Narrow-band imaging. In: Wayne JD, Rex DK, Williams CB (eds) Colonoscopy: principles and practice, 2nd edn., pp. 514–526. http://onlinelibrary.wiley.com/doi/10.1002/9781444316902.ch38/summary
3. Nayar SK, Krishnan G, Grossberg MD, Raskar R (2006) Fast separation of direct and global components of a scene using high frequency illuminationm In: ACM SIGGRAPH 2006 papers on-SIGGRAPH '06, pp. 935–944
4. Tanaka K, Mukaigawa Y, Kubo H, Matsushita Y, Yagi Y (2015) Recovering inner slices of translucent objects by multi-frequency illumination. In: The IEEE conference on computer vision and pattern recognition, pp. 5464–5472
5. Hayakawa Y, Yamashita H, Otsuburai T, Miyoseta Y, Sagawa M, Kondo A, Tsuji Y, Honda A (2010) Near-infrared radiation imaging for the detection of alien substances under the skin. Med. Imaging Inf. Sci. 27(3):50–54
6. Nishida K, Namita T, Kato Y, Shimizu K (2012) Improvement of transillumination image of blood vessels using multiple wavelengths of light. IEICE Tech. Rep. MBE2011-111 111(482):13–18
7. Elhawary H, Popovic A (2011) Robust feature tracking on the beating heart for a robotic-guided endoscope. Int J Med Robot Comput Assist Surg 7:459–468
8. Bay H, Tuytelaars T, Gool LV (2006) SURF: speeded up robust features. Lecture Notes in Computer Science, vol. 3951 LNCS, pp. 404–417

9. Tomasi C (1991) Detection and Tracking of Point Features. Tech Rep CMU-CS-91-132 Image Rochester 91:1–22
10. Haouchine N, Dequidt J, Peterlik I, Kerrien E, Berger M (2013) Image-guided simulation of heterogeneous tissue deformation for augmented reality during hepatic surgery. In: 2013 IEEE international symposium on mixed and augmented reality, pp. 199–208
11. Lowe DG (2004) Distinctive image features from scale-invariant keypoints. Int J Comput Vis 60(2):91–110
12. Rosten E, Drummond T (2006) Machine learning for high-speed corner detection. In: Computer vision—ECCV 2006, vol 3951. Springer, Berlin, Heidelberg, pp 430–443
13. Puerto-Souza GA, Mariottini GL (2012) Hierarchical multi-affine (HMA) algorithm for fast and accurate feature matching in minimally-invasive surgical images. In: 2012 IEEE/RSJ international conference on intelligent robots and systems (IROS), pp. 2007–2012
14. Ling H, David WJ (2005) Deformation invariant image matching. In: Tenth IEEE international conference on computer vision, 2005. ICCV 2005, vol. 2, pp. 1466–1473
15. Lobaton E, Vasudevan R, Alterovitz R, Bajcsy R (2011) Robust topological features for deformation invariant image matching. In: 2011 IEEE international conference on computer vision (ICCV), pp. 2516–2523